CLOSED-FORM SOLUTIONS FOR PREDICTING INTERLAMINAR SHEAR STRESS AND HYGROTHERMOMECHANICAL NORMAL STRESS IN COMPOSITE BEAMS WITH RECTANGULAR AND TUBULAR CROSS-SECTIONS

Sthanu Mahadev[1*], Wen Chan[2], Taylor Best[1], Reiley Schraeger[1]

California Polytechnic State University[1]
San Luis Obispo, California-USA

The University of Texas at Arlington[2]

ABSTRACT

Closed-form analytical solutions for thin-walled laminated composite beams with tubular and rectangular cross-sections are developed for evaluating interlaminar shear stress and thermally induced stresses. The formulations are fundamentally based on modified Composite lamination theory and parallel axis theorem. The present approach includes a variation of ply stiffness along the contour of the cross-section. Interlaminar shear stresses in cantilevered composite beams with rectangular cross-section under a transverse load is analytically determined to be independent of a temperature differential subjected to uniform temperature environment. An ANSYS based three-dimensional finite element model for computing thermal stresses of both cross-sections is further demonstrated. The results obtained from analytical solutions give an excellent agreement to finite element results. This mathematical model represents an efficient tool for structural design engineers to perform parametric studies during the preliminary design phase.

Keywords: Thin-walled, composite beams, Composite Lamination Theory.

1. INTRODUCTION

Over the last decades, fiber-reinforced composite materials have played an increasingly significant role in numerous aerospace structural applications and continue to represent the preferred material option due to superior specific mechanical properties such as stiffness-to-weight ratio, low-density characteristics, coupled with significant improvements in fatigue resistance compared to metal structure counterparts [1]. Fiber-reinforced composite laminates in the form of tubular structures have witnessed numerous applications in aerospace, civil structure, sporting and automobile industries.

Extensive research efforts have been devoted in recent years towards the development of efficient thin-walled structural members such as composite tubes, columns, and beams. Accurate evaluation of primary mechanical properties such as axial stiffness, bending stiffness and ply stresses are warranted to achieve a conceptual understanding of structural response to deformations, loads and mechanical vibrations [1]. Considerable work has been performed towards understanding the structural response of laminated composite cylinders under various loading conditions. Whitney [2,3,4] studied the structural response of cylindrical (curved) plates under bending, buckling and mechanically induced vibrations. Vinson and Sierakowski [5] investigated the buckling behavior on circular composite shell structures.

Recently, Hoa [6], in his book, extends classical lamination theory to cylindrical composite shell for fiber reinforced plastic vessels and piping application. Theoretical estimations based on thin-walled composite beam theory were published in the book written by Librescu and Song [7]. Among that technical literature, the influence of fiber-orientation angle along the tube circumference was not considered. Recently, Mahadev and Chan .et al [8, 9] developed a simple closed-form expression for evaluating bending stiffness of laminated composite tubes. Influence of curvature effect on bending stiffness was investigated by conducting a parametric study on tubes of varying radius and. Bending stiffness predictions based on laminate shell theory analytical model proved to be more accurate compared to the laminate plate approach. Mahadev, Hanze and Chan [10] extended the former tube model to analyze laminated composite cylindrical shells subject to a hygrothermomechanical environment. The obtained analytical results show an excellent agreement with finite element method results. Rao [11] has developed closed-form expressions based on modifying the laminated plate approach to determine the displacement and twisting angle of the tapered composite tube under axial tension and torsion. Sims and Wilson [12] have derived an approximate elasticity solution for the transverse shearing stresses in a multilayered anisotropic composite beam. The distribution of shear stresses through the laminate thickness obtained from analytical solution has been validated by experimental data. Syed and Chan [13] have developed an analytical model to analyze the bending stiffness matrices for a laminated composite beam with hat cross-section. The thermally induced ply stresses and the location of the centroid and shear center of the hat sectional composite beam have also been included in his study.

Other researches have been focused on induced stresses between and within laminas while laminated composite structures are subjected to temperature change. Boley and Weiner [14] describe the general theory of thermal stresses of beam structures in their published book. Using finite element method to analyze the behavior of laminated composite structure under temperature environment is one of the common approaches. Naidu and Sinha [15] have studied the large deflection and bending behavior of composite cylindrical shell panels subjected to the hygrothermal environment using nonlinear finite element analysis. Seibi and Amatcau [16] have researched on the use of the laminated plate theory (LPT) to optimize the architecture of laminated ceramic matrix composite tube processing high thermal cracking resistance. They have developed a method to estimate the induced thermal residual stresses of a laminated composite tube under significant temperature change using finite element modeling program ANSYS. Shariyat [17] has studied for thermal buckling analysis of a rectangular composite multilayered plate under uniform temperature rise using a layer-wise plate theory to determine the buckling temperature. However, finite element analysis is still not an efficient method because of structural configuration dependent. Hence, some other efforts have been made on developing analytical models and closed-form expressions for thermal analysis of composite laminates. Kim, B., Kim, T., Byun, and Lee [18] have derived a closed-form solution for composite/ceramic tube to calculate the shrink fit stresses, the stresses due to internal pressure and thermal stresses due to temperature differences between the inside and outside of the tube. Khdeir [19] has developed an exact analytical solution of refined beam theories to obtain the critical buckling temperature of a cross-ply beam subjected to uniform temperature distribution with various boundary conditions. Additionally, Syed, Su, and Chan [20] have presented simple analytical expressions for computing thermal stresses in fiber reinforced composite beam with rectangular and hat cross-sections under uniform temperature environment. In-plane stresses and interlaminar shear stress were also analyzed. For designing composite beam structure, the developing of analytical method not only provide an accurate evaluation of sectional properties for better prediction of structure behaviors but also can be much easier used for a parametric study.

In the present research, the primary objective is to develop closed-form solutions for a laminated composite circular tube, and rectangular beam to determine their hygrothermally induced load and moment matrices based on modified lamination theory, parallel axis theorem, and laminated plate approach [1, 8, and 10]. In-plane stresses and interlaminar shear stresses through the thickness of the laminate are also investigated. Results are compared and validated by performing finite element analysis of fully three-dimensional constructed models. The finite element models are developed in the commercial software package ANSYS and verified by first applying properties of isotropic material on them. In this study, the composite material Carbon/Epoxy AS4/3501-6 [21,22, 23] is chosen for both cases. Additionally, the parametric studies are conducted to study the stacking sequence and fiber orientation effects on the thermally induced in-plane axial and interlaminar shear stresses.

2. ANALYTICAL SOLUTION DEVELOPMENT FOR THIN-WALLED RECTANGULAR COMPOSITE BEAMS UNDER HYGROTHEROMECHANICAL ENVIRONMENT

2.1 Interlaminar Shear Stress Formulation for Composite Beams subject to Transverse Shear Load

The composite beam under investigation is assumed to constitute a rectangular cross-section beam with width, d and the height, h. The length, L of the composite beam is assumed to be significantly longer than its width and height. In all the derivations, the cross-sectional plane of the beam is assumed to remain plane before and after deformation. In other words, Bernoulli's hypothesis is preserved. Each individual lamina constituting the composite beam laminate is assumed to be under a plane stress type-loading environment. This means that stresses such as $\sigma_z, \tau_{xz} and \tau_{yz}$ are assumed to be zero for this analysis. As a consequence, interlaminar shear stress components may not be obtained directly from composite lamination theory. However, these stresses are procured from equations of equilibrium as shown in Eq.1. Development of interlaminar shear stresses $\tau_{xz} and \tau_{yz}$ and normal stress σ_z due to edge effects are ignored.

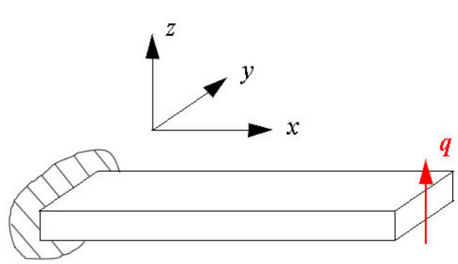

Fig. 1. Laminated Composite Beam Schematic under Transverse Load

The equations of equilibrium for any arbitrary layer k within the laminate is given by:

$$\begin{aligned}
&\frac{\partial \sigma_x^k}{\partial x}+\frac{\partial \tau_{xy}^k}{\partial y}+\frac{\partial \tau_{xz}^k}{\partial z}=0\\
&\frac{\partial \tau_{yx}^k}{\partial x}+\frac{\partial \sigma_y^k}{\partial y}+\frac{\partial \tau_{yz}^k}{\partial z}=0\\
&\frac{\partial \tau_{xz}^k}{\partial x}+\frac{\partial \tau_{yz}^k}{\partial y}+\frac{\partial \sigma_z^k}{\partial z}=0
\end{aligned} \tag{1}$$

Additionally, since the beam is assumed to be narrow, the stresses are assumed to be independent of y-direction, Eq. (1) can be represented as:

$$\begin{aligned}
&\frac{\partial \sigma_x^k}{\partial x}+\frac{\partial \tau_{xz}^k}{\partial z}=0\\
&\tau_{xz}^k=-\int_{z_{k-1}}^{z_k}\frac{\partial \sigma_x^k}{\partial x}.dz+\tau_{xz}^{k-1}
\end{aligned} \tag{2}$$

For a multi-layered laminate with the mid-plane interlaminar stress $\tau_{xz}^{o}=0$, Eqn. (2) reduces to

$$\tau_{xz}^k=-\sum_{i=1}^{k}\int_{z_{k-1}}^{z_k}\frac{\partial \sigma_x^i}{\partial x}.dz \tag{3}$$

Based on the conventional lamination theory, the laminated constitutive equation including thermal effect is given as:

$$\begin{aligned}
&\begin{pmatrix}\overline{N}+N^T+N^H\\ \overline{M}+M^T+M^H\end{pmatrix}=\begin{pmatrix}A & B\\ B & D\end{pmatrix}*\begin{pmatrix}\varepsilon_0\\ \kappa\end{pmatrix}\\
&\begin{pmatrix}\varepsilon_0\\ \kappa\end{pmatrix}=\begin{pmatrix}a & b\\ b^T & d\end{pmatrix}*\begin{pmatrix}\overline{N}+N^T+N^H\\ \overline{M}+M^T+M^H\end{pmatrix}
\end{aligned} \tag{4}$$

Since the cantilevered rectangular beam is under a transverse shear load, q, the in-plane forces are not considered on the beam. Furthermore, in this derivation, the cantilever beam is assumed to behave as a narrow beam. Hence, we have:

$$\begin{aligned}
&N_x=N_y=N_{xy}=M_y=M_{xy}=0\\
&\text{and}\\
&\frac{\partial M_x}{\partial x}=-q
\end{aligned} \tag{5}$$

Where, q is the transversely applied shear load per unit width. Then Eqn. (4) can be modified as

$$\begin{aligned}
&\left\{\varepsilon^0\right\}=[a].[N^T+N^H]+[b].[M+M^T+M^H]\\
&\left\{\kappa^0\right\}=[b].[N^T+N^H]+[d].[M+M^T+M^H]
\end{aligned} \tag{6}$$

Substituting Eq. (5) and Eq. (6) into Eq. (3) we get:

$$\tau_{xz}^{k} = -\sum_{i=1}^{k} \int_{z_{k-1}}^{z_k} \frac{\partial \sigma_x^i}{\partial x}.dz$$

$$\tau_{xz}^{k} = -\sum_{i=1}^{N} \int_{z_{k-1}}^{z_k} \left(\begin{array}{l} \left\{ \overline{Q}_{11}^{\,k}.\left(\frac{\partial \varepsilon_x^0}{\partial x} + z_k \frac{\partial \kappa_x^0}{\partial x} - \frac{\partial \alpha_x}{\partial x}\Delta T - \frac{\partial \beta_x}{\partial x}\Delta C \right) \right\} + \\ \left\{ \overline{Q}_{21}^{\,k}.\left(\frac{\partial \varepsilon_y^0}{\partial x} + z_k \frac{\partial \kappa_y^0}{\partial x} - \frac{\partial \alpha_y}{\partial x}\Delta T - \frac{\partial \beta_y}{\partial x}\Delta C \right) \right\} \\ + \left\{ \overline{Q}_{61}^{\,k}.\left(\frac{\partial \gamma_{xy}^0}{\partial x} + z_k \frac{\partial \kappa_{xy}^0}{\partial x} - \frac{\partial \alpha_{xy}}{\partial x}\Delta T - \frac{\partial \beta_{xy}}{\partial x}\Delta C \right) \right\} \end{array} \right).dz \tag{7}$$

Since $\left[N^T, N^H\right] and \left[M^T, M^H\right]$ does not depend on cross-sectional dimension of the composite beam, their partial derivatives are excluded. Eqn. (7) can be reduced as:

$$\tau_{xz}^{k} = -\sum_{i=1}^{N} \int_{z_{k-1}}^{z_k} \left(\begin{array}{l} \left\{ \overline{Q}_{11}^{\,k}.\left((-b_{11}.q) + z_k(-d_{11}.q) \right) \right\} + \\ \left\{ \overline{Q}_{21}^{\,k}.\left((-b_{21}.q) + z_k(-d_{21}.q) \right) \right\} \\ + \left\{ \overline{Q}_{61}^{\,k}.\left((-b_{61}.q) + z_k(-d_{61}.q) \right) \right\} \end{array} \right).dz$$

$$\tau_{xz}^{k} = -\sum_{i=1}^{N} \int_{z_{k-1}}^{z_k} \left(\begin{array}{l} \left\{ \overline{Q}_{11}^{\,k}.\left((-b_{11}) + z_k(-d_{11}) \right) \right\} + \\ \left\{ \overline{Q}_{21}^{\,k}.\left((-b_{21}) + z_k(-d_{21}) \right) \right\} \\ + \left\{ \overline{Q}_{61}^{\,k}.\left((-b_{61}) + z_k(-d_{61}) \right) \right\} \end{array} \right).q.dz \tag{8}$$

$$\tau_{xz}^{k} = -\sum_{i=1}^{N} \int_{z_{k-1}}^{z_k} \left(\begin{array}{l} \left\{ \overline{Q}_{11}^{\,k}.\left((-b_{11}) + z_k(-d_{11}) \right) \right\} + \\ \left\{ \overline{Q}_{21}^{\,k}.\left((-b_{21}) + z_k(-d_{21}) \right) \right\} \\ + \left\{ \overline{Q}_{61}^{\,k}.\left((-b_{61}) + z_k(-d_{61}) \right) \right\} \end{array} \right).q.dz \tag{9}$$

$$\tau_{xz}^{k} = q.\left\{ \sum_{i=1}^{N} QB_i(z_k - z_{k-1}) + \frac{1}{2}\sum_{i=1}^{N} QD_i(z_k^2 - z_{k-1}^2) \right\}$$

Eqs.(8) and (9) represents the closed-form expression for interlaminar shear stress τ_{xz} for a thin-walled narrow type rectangular composite beam. The expression shows that τ_{xz} is primarily a function of the applied transverse shear load, reduced laminate stiffness, and compliance terms respectively. Additionally, the expression indicates that hygrothermally induced forces and moments do have any influence on the resultant interlaminar shear stress under an externally applied transverse shear load.

3. ANALYTICAL SOLUTION DEVELOPMENT FOR THIN-WALLED TUBULAR COMPOSITE BEAMS UNDER HYGROTHERMOMECHANICAL ENVIRONMENT

Two analytical methods, laminated plate approach, and laminated shell approach, for evaluating stiffness matrices of the circular composite tube were developed by Chan and Demirhan [1]. Plate approach is chosen here because of its simplicity. Both of these two approaches were derived based on the conventional lamination theory and translation of laminate axis.

In this approach, an infinitesimal plate element of the laminated composite tube (Fig.2) is considered. The infinitesimal element, which is inclined an angle, θ, with respect to the axis of the tube, z, is rotated about the x'' axis as shown in Fig. 3. Thus, the reduced stiffness matrix of lamina, [Q] needs to be first transformed about x'' axis with an angle, θ, then transformed about z' axis with the angle of fiber orientation of the ply.

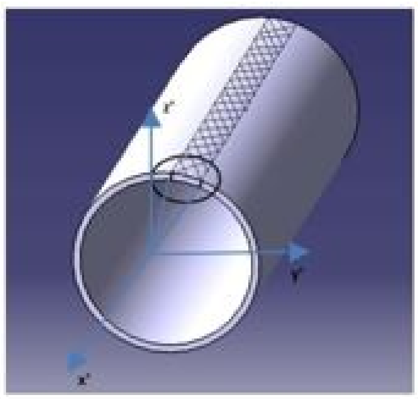

Fig. 2. Laminated Tube Schematic

An infinitesimal plate element (Fig. 3) is focused on in deriving the stiffness matrices utilizing laminated plate approach. The hygrothermally induced force and moment of the element are obtained by integrating hygrothermal strains through the thickness of lamina, and can be written as:

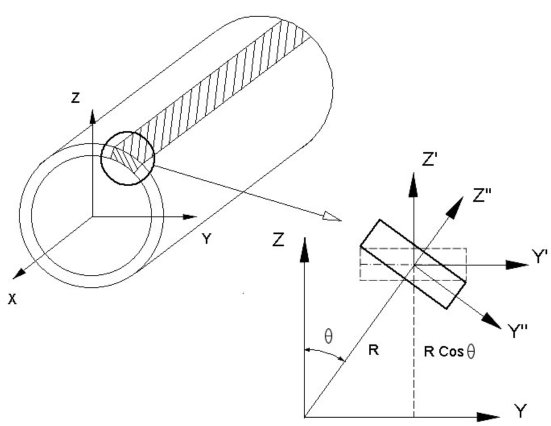

Fig.3. Infinitesimal Plate Element from a Thin-walled Composite Beam

$$
\begin{aligned}
N^{T}_{x'} &= \Delta T.\sum_{k=1}^{N}\left(\hat{Q}^{k}_{11}.\alpha^{k}_{x}+\hat{Q}^{k}_{12}.\alpha^{k}_{y}+\hat{Q}^{k}_{16}.\alpha^{k}_{xy}\right).\left(z'_{k}-z'_{k-1}\right)\\
N^{H}_{x'} &= \Delta C.\sum_{k=1}^{N}\left(\hat{Q}^{k}_{11}.\alpha^{k}_{x}+\hat{Q}^{k}_{12}.\alpha^{k}_{y}+\hat{Q}^{k}_{16}.\alpha^{k}_{xy}\right).\left(z'_{k}-z'_{k-1}\right)\\
N^{T}_{y'} &= \Delta T.\sum_{k=1}^{N}\left(\hat{Q}^{k}_{21}.\alpha^{k}_{x}+\hat{Q}^{k}_{22}.\alpha^{k}_{y}+\hat{Q}^{k}_{26}.\alpha^{k}_{xy}\right).\left(z'_{k}-z'_{k-1}\right)\\
N^{H}_{y'} &= \Delta C.\sum_{k=1}^{N}\left(\hat{Q}^{k}_{21}.\alpha^{k}_{x}+\hat{Q}^{k}_{22}.\alpha^{k}_{y}+\hat{Q}^{k}_{26}.\alpha^{k}_{xy}\right).\left(z'_{k}-z'_{k-1}\right)\\
N^{T}_{xy'} &= \Delta T.\sum_{k=1}^{N}\left(\hat{Q}^{k}_{61}.\alpha^{k}_{x}+\hat{Q}^{k}_{62}.\alpha^{k}_{y}+\hat{Q}^{k}_{66}.\alpha^{k}_{xy}\right).\left(z'_{k}-z'_{k-1}\right)\\
N^{H}_{xy'} &= \Delta C.\sum_{k=1}^{N}\left(\hat{Q}^{k}_{61}.\alpha^{k}_{x}+\hat{Q}^{k}_{62}.\alpha^{k}_{y}+\hat{Q}^{k}_{66}.\alpha^{k}_{xy}\right).\left(z'_{k}-z'_{k-1}\right)
\end{aligned}
\tag{10}
$$

Where, $\hat{Q}^{k}_{ij}$ is the transformed reduced stiffness matrix, and ΔT is the change of the temperature. $[N^{T}_{x,y,xy}],\left[N^{H}_{x,y,xy}\right]$ represent the thermal and hygric force components in the elemental rotated coordinated system. $[M^{T}_{x,y,xy}],\left[M^{H}_{x,y,xy}\right]$ represent the thermal and hygric force components in the elemental rotated coordinated system.

The forces and moments obtained using Eqn. (15) and Eqn. (16) act along the mid-plane of the lamina. In order to transfer these resultants to the reference axis of the tube structure, concepts of parallel axis theorem are applied. In the present case, as shown in Fig.3, the distance from new reference axis to the original axis, d is assumed to be $R_m\text{Cos}\theta$. Then, the hygrothermally induced thermal induced force and moment per unit width of the tube can be shown as:

(11)

$$
\begin{aligned}
M^{T}_{x'} &= \frac{\Delta T}{2}.\sum_{k=1}^{N}\left(\hat{Q}^{k}_{11}.\alpha^{k}_{x}+\hat{Q}^{k}_{12}.\alpha^{k}_{y}+\hat{Q}^{k}_{16}.\alpha^{k}_{xy}\right).\left(z^{2'}_{k}-z^{2}_{k-1}{}'\right)\\
M^{H}_{x'} &= \frac{\Delta C}{2}.\sum_{k=1}^{N}\left(\hat{Q}^{k}_{11}.\alpha^{k}_{x}+\hat{Q}^{k}_{12}.\alpha^{k}_{y}+\hat{Q}^{k}_{16}.\alpha^{k}_{xy}\right).\left(z^{2'}_{k}-z^{2}_{k-1}{}'\right)\\
M^{T}_{y'} &= \frac{\Delta T}{2}.\sum_{k=1}^{N}\left(\hat{Q}^{k}_{21}.\alpha^{k}_{x}+\hat{Q}^{k}_{22}.\alpha^{k}_{y}+\hat{Q}^{k}_{26}.\alpha^{k}_{xy}\right).\left(z^{2'}_{k}-z^{2}_{k-1}{}'\right)\\
M^{H}_{y'} &= \frac{\Delta C}{2}.\sum_{k=1}^{N}\left(\hat{Q}^{k}_{21}.\alpha^{k}_{x}+\hat{Q}^{k}_{22}.\alpha^{k}_{y}+\hat{Q}^{k}_{26}.\alpha^{k}_{xy}\right).\left(z^{2'}_{k}-z^{2}_{k-1}{}'\right)\\
M^{T}_{xy'} &= \frac{\Delta T}{2}.\sum_{k=1}^{N}\left(\hat{Q}^{k}_{61}.\alpha^{k}_{x}+\hat{Q}^{k}_{62}.\alpha^{k}_{y}+\hat{Q}^{k}_{66}.\alpha^{k}_{xy}\right).\left(z^{2'}_{k}-z^{2}_{k-1}{}'\right)\\
M^{H}_{xy'} &= \frac{\Delta C}{2}.\sum_{k=1}^{N}\left(\hat{Q}^{k}_{61}.\alpha^{k}_{x}+\hat{Q}^{k}_{62}.\alpha^{k}_{y}+\hat{Q}^{k}_{66}.\alpha^{k}_{xy}\right).\left(z^{2'}_{k}-z^{2}_{k-1}{}'\right)
\end{aligned}
\tag{12}
$$

$$N_x^T = \Delta T.\sum_{k=1}^{N}\left(\hat{Q}_{11}^k.\alpha_x^k + \hat{Q}_{12}^k.\alpha_y^k + \hat{Q}_{16}^k.\alpha_{xy}^k\right).\left[\left(\left(z'_k + R_m.\mathrm{Cos}\theta\right) - \left(z'_{k-1} + R_m.\mathrm{Cos}\theta\right)\right)\right] = N_{x'}^T$$

$$N_x^H = \Delta C.\sum_{k=1}^{N}\left(\hat{Q}_{11}^k.\alpha_x^k + \hat{Q}_{12}^k.\alpha_y^k + \hat{Q}_{16}^k.\alpha_{xy}^k\right).\left[\left(\left(z'_k + R_m.\mathrm{Cos}\theta\right) - \left(z'_{k-1} + R_m.\mathrm{Cos}\theta\right)\right)\right] = N_{x'}^H$$

$$N_y^T = \Delta T.\sum_{k=1}^{N}\left(\hat{Q}_{21}^k.\alpha_x^k + \hat{Q}_{22}^k.\alpha_y^k + \hat{Q}_{26}^k.\alpha_{xy}^k\right).\left[\left(\left(z'_k + R_m.\mathrm{Cos}\theta\right) - \left(z'_{k-1} + R_m.\mathrm{Cos}\theta\right)\right)\right] = N_{y'}^T$$

$$N_y^H = \Delta C.\sum_{k=1}^{N}\left(\hat{Q}_{21}^k.\alpha_x^k + \hat{Q}_{22}^k.\alpha_y^k + \hat{Q}_{26}^k.\alpha_{xy}^k\right).\left[\left(\left(z'_k + R_m.\mathrm{Cos}\theta\right) - \left(z'_{k-1} + R_m.\mathrm{Cos}\theta\right)\right)\right] = N_{y'}^H \qquad (13)$$

$$N_{xy}^T = \Delta T.\sum_{k=1}^{N}\left(\hat{Q}_{61}^k.\alpha_x^k + \hat{Q}_{62}^k.\alpha_y^k + \hat{Q}_{66}^k.\alpha_{xy}^k\right).\left[\left(\left(z'_k + R_m.\mathrm{Cos}\theta\right) - \left(z'_{k-1} + R_m.\mathrm{Cos}\theta\right)\right)\right] = N_{xy'}^T$$

$$N_{xy}^H = \Delta C.\sum_{k=1}^{N}\left(\hat{Q}_{61}^k.\alpha_x^k + \hat{Q}_{62}^k.\alpha_y^k + \hat{Q}_{66}^k.\alpha_{xy}^k\right).\left[\left(\left(z'_k + R_m.\mathrm{Cos}\theta\right) - \left(z'_{k-1} + R_m.\mathrm{Cos}\theta\right)\right)\right] = N_{xy'}^H$$

To obtain the overall thermal induced force and moment of the composite circular tube, Eqn. (17) and Eqn. (18) expressed above needs to be integrated over the entire length of the circumference of the tube. They can be re-expressed as:

$$\left[\overline{N}_X^T\right] = \int_0^{2\pi} N_x^T * R_m.d\theta$$

$$= \int_0^{2\pi} \Delta T.\sum_{k=1}^{N}\left(\hat{Q}_{11}^k.\alpha_x^k + \hat{Q}_{12}^k.\alpha_y^k + \hat{Q}_{16}^k.\alpha_{xy}^k\right).\left[\left(\left(z'_k + R_m.\mathrm{Cos}\theta\right) - \left(z'_{k-1} + R_m.\mathrm{Cos}\theta\right)\right)\right] R_m.d\theta$$

$$= \pi.R_m.\Delta T.\left\{\begin{matrix}\left(\mathrm{Cos}\,\theta_z^6 + \mathrm{Sin}\,\theta_z^4\,\mathrm{Cos}\,\theta_z^2 + 2\mathrm{Sin}\,\theta_z^2\,\mathrm{Cos}\,\theta_z^4\right)\left(2Q_{11}\alpha_1 + \frac{3}{4}Q_{12}\alpha_2\right) + \\ \left(\mathrm{Sin}\,\theta_z^6 + \mathrm{Sin}\,\theta_z^2\,\mathrm{Cos}\,\theta_z^4 + 2\mathrm{Sin}\,\theta_z^4\,\mathrm{Cos}\,\theta_z^2\right)\left(Q_{12}\alpha_1 + \frac{5}{8}Q_{22}\alpha_2\right)\end{matrix}\right\}.\left(z'_k - z'_{k-1}\right)$$

$$\left[\overline{N}_X^H\right] = \int_0^{2\pi} N_x^H * R_m.d\theta$$

$$= \int_0^{2\pi} \Delta C.\sum_{k=1}^{N}\left(\hat{Q}_{11}^k.\alpha_x^k + \hat{Q}_{12}^k.\alpha_y^k + \hat{Q}_{16}^k.\alpha_{xy}^k\right).\left[\left(\left(z'_k + R_m.\mathrm{Cos}\theta\right) - \left(z'_{k-1} + R_m.\mathrm{Cos}\theta\right)\right)\right] R_m.d\theta$$

$$= \pi.R_m.\Delta C.\left\{\begin{matrix}\left(\mathrm{Cos}\,\theta_z^6 + \mathrm{Sin}\,\theta_z^4\,\mathrm{Cos}\,\theta_z^2 + 2\mathrm{Sin}\,\theta_z^2\,\mathrm{Cos}\,\theta_z^4\right)\left(2Q_{11}\alpha_1 + \frac{3}{4}Q_{12}\alpha_2\right) + \\ \left(\mathrm{Sin}\,\theta_z^6 + \mathrm{Sin}\,\theta_z^2\,\mathrm{Cos}\,\theta_z^4 + 2\mathrm{Sin}\,\theta_z^4\,\mathrm{Cos}\,\theta_z^2\right)\left(Q_{12}\alpha_1 + \frac{5}{8}Q_{22}\alpha_2\right)\end{matrix}\right\}.\left(z'_k - z'_{k-1}\right) \qquad (14)$$

$$\left[\overline{N}_y^T\right]=\int_0^{2\pi} N_y^T * R_m.d\theta$$

$$=\int_0^{2\pi}\Delta T.\sum_{k=1}^{N}\left(\hat{Q}_{21}^k.\alpha_x^k+\hat{Q}_{22}^k.\alpha_y^k+\hat{Q}_{26}^k.\alpha_{xy}^k\right).\left[\left(\left(z'_k+R_m.\mathrm{Cos}\theta\right)-\left(z'_{k-1}+R_m.\mathrm{Cos}\theta\right)\right)\right]$$

$$=\pi.R_m.\Delta T.\begin{Bmatrix}\left(\mathrm{Sin}\,\theta_z^6+\mathrm{Sin}\,\theta_z^2\,\mathrm{Cos}\,\theta_z^4+2\mathrm{Sin}\,\theta_z^4\,\mathrm{Cos}\,\theta_z^2\right)\left(2Q_{11}\alpha_1+\frac{3}{4}Q_{12}\alpha_2\right)+\\ \left(\mathrm{Cos}\,\theta_z^6+\mathrm{Sin}\,\theta_z^4\,\mathrm{Cos}\,\theta_z^2+2\mathrm{Sin}\,\theta_z^2\,\mathrm{Cos}\,\theta_z^4\right)\left(Q_{12}\alpha_1+\frac{5}{8}Q_{22}\alpha_2\right)\end{Bmatrix}.\left(z'_k-z'_{k-1}\right)$$

$$\left[\overline{N}_y^H\right]=\int_0^{2\pi} N_y^H * R_m.d\theta$$

$$=\int_0^{2\pi}\Delta C.\sum_{k=1}^{N}\left(\hat{Q}_{21}^k.\alpha_x^k+\hat{Q}_{22}^k.\alpha_y^k+\hat{Q}_{26}^k.\alpha_{xy}^k\right).\left[\left(\left(z'_k+R_m.\mathrm{Cos}\theta\right)-\left(z'_{k-1}+R_m.\mathrm{Cos}\theta\right)\right)\right]$$

$$=\pi.R_m.\Delta C.\begin{Bmatrix}\left(\mathrm{Sin}\,\theta_z^6+\mathrm{Sin}\,\theta_z^2\,\mathrm{Cos}\,\theta_z^4+2\mathrm{Sin}\,\theta_z^4\,\mathrm{Cos}\,\theta_z^2\right)\left(2Q_{11}\alpha_1+\frac{3}{4}Q_{12}\alpha_2\right)+\\ \left(\mathrm{Cos}\,\theta_z^6+\mathrm{Sin}\,\theta_z^4\,\mathrm{Cos}\,\theta_z^2+2\mathrm{Sin}\,\theta_z^2\,\mathrm{Cos}\,\theta_z^4\right)\left(Q_{12}\alpha_1+\frac{5}{8}Q_{22}\alpha_2\right)\end{Bmatrix}.\left(z'_k-z'_{k-1}\right) \tag{15}$$

$$\left[\overline{N}_{XY}^T\right]=\int_0^{2\pi} N_{xy}^T * R_m.d\theta$$

$$=\int_0^{2\pi}\Delta T.\sum_{k=1}^{N}\left(\hat{Q}_{61}^k.\alpha_x^k+\hat{Q}_{62}^k.\alpha_y^k+\hat{Q}_{66}^k.\alpha_{xy}^k\right).\left[\left(\left(z'_k+R_m.\mathrm{Cos}\theta\right)-\left(z'_{k-1}+R_m.\mathrm{Cos}\theta\right)\right)\right]R_m.d\theta$$

$$=\pi.R_m.\Delta T.\begin{Bmatrix}\left(\mathrm{Sin}\,\theta\,\mathrm{Cos}\,\theta_z^5+\mathrm{Sin}\,\theta_z^5\,\mathrm{Cos}\,\theta_z+2\mathrm{Sin}\,\theta_z^3\,\mathrm{Cos}\,\theta_z^3\right)\left(2Q_{11}\alpha_1-Q_{12}\alpha_1\right)+\\ \left(\mathrm{Sin}\,\theta\,\mathrm{Cos}\,\theta_z^5+\mathrm{Sin}\,\theta_z^5\,\mathrm{Cos}\,\theta_z+2\mathrm{Sin}\,\theta_z^3\,\mathrm{Cos}\,\theta_z^3\right)\left(\frac{3}{4}Q_{12}\alpha_2-\frac{5}{8}Q_{22}\alpha_2\right)\end{Bmatrix}.\left(z'_k-z'_{k-1}\right)$$

(16)

$$\left[\overline{N}_{XY}^H\right]=\int_0^{2\pi} N_{xy}^H * R_m.d\theta$$

$$=\int_0^{2\pi}\Delta C.\sum_{k=1}^{N}\left(\hat{Q}_{61}^k.\alpha_x^k+\hat{Q}_{62}^k.\alpha_y^k+\hat{Q}_{66}^k.\alpha_{xy}^k\right).\left[\left(\left(z'_k+R_m.\mathrm{Cos}\theta\right)-\left(z'_{k-1}+R_m.\mathrm{Cos}\theta\right)\right)\right]R_m.d\theta$$

$$=\pi.R_m.\Delta C.\begin{Bmatrix}\left(\mathrm{Sin}\,\theta\,\mathrm{Cos}\,\theta_z^5+\mathrm{Sin}\,\theta_z^5\,\mathrm{Cos}\,\theta_z+2\mathrm{Sin}\,\theta_z^3\,\mathrm{Cos}\,\theta_z^3\right)\left(2Q_{11}\alpha_1-Q_{12}\alpha_1\right)+\\ \left(\mathrm{Sin}\,\theta\,\mathrm{Cos}\,\theta_z^5+\mathrm{Sin}\,\theta_z^5\,\mathrm{Cos}\,\theta_z+2\mathrm{Sin}\,\theta_z^3\,\mathrm{Cos}\,\theta_z^3\right)\left(\frac{3}{4}Q_{12}\alpha_2-\frac{5}{8}Q_{22}\alpha_2\right)\end{Bmatrix}.\left(z'_k-z'_{k-1}\right)$$

$$\left[\overline{M}_X^T\right] = \int_0^{2\pi} M_x^T * R_m.d\theta$$

$$= \int_0^{2\pi} \frac{\Delta T}{2}.\sum_{k=1}^{N}\left(\hat{Q}_{11}^k.\alpha_x^k + \hat{Q}_{12}^k.\alpha_y^k + \hat{Q}_{16}^k.\alpha_{xy}^k\right).\left[\left(\left(z'_k + R_m.\mathrm{Cos}\,\theta\right)^2 - \left(z'_{k-1} + R_m.\mathrm{Cos}\,\theta\right)^2\right)\right]R_m.d\theta$$

$$= \frac{\pi.R_m.\Delta T}{2}.\left\{\begin{array}{l}\left(\mathrm{Cos}\,\theta_z^6 + \mathrm{Sin}\,\theta_z^4\,\mathrm{Cos}\,\theta_z^2 + 2\mathrm{Sin}\,\theta_z^2\,\mathrm{Cos}\,\theta_z^4\right)\left(2Q_{11}\alpha_1 + \frac{3}{4}Q_{12}\alpha_2\right) + \\ \left(\mathrm{Sin}\,\theta_z^6 + \mathrm{Sin}\,\theta_z^2\,\mathrm{Cos}\,\theta_z^4 + 2\mathrm{Sin}\,\theta_z^4\,\mathrm{Cos}\,\theta_z^2\right)\left(Q_{12}\alpha_1 + \frac{5}{8}Q_{22}\alpha_2\right)\end{array}\right\}.\left(z_k^{2'} - z_{k-1}^{2}{}'\right)$$

$$\left[\overline{M}_X^H\right] = \int_0^{2\pi} M_x^H * R_m.d\theta$$

$$= \int_0^{2\pi} \frac{\Delta C}{2}.\sum_{k=1}^{N}\left(\hat{Q}_{11}^k.\alpha_x^k + \hat{Q}_{12}^k.\alpha_y^k + \hat{Q}_{16}^k.\alpha_{xy}^k\right).\left[\left(\left(z'_k + R_m.\mathrm{Cos}\,\theta\right)^2 - \left(z'_{k-1} + R_m.\mathrm{Cos}\,\theta\right)^2\right)\right]R_m.d\theta$$

$$= \frac{\pi.R_m.\Delta C}{2}.\left\{\begin{array}{l}\left(\mathrm{Cos}\,\theta_z^6 + \mathrm{Sin}\,\theta_z^4\,\mathrm{Cos}\,\theta_z^2 + 2\mathrm{Sin}\,\theta_z^2\,\mathrm{Cos}\,\theta_z^4\right)\left(2Q_{11}\alpha_1 + \frac{3}{4}Q_{12}\alpha_2\right) + \\ \left(\mathrm{Sin}\,\theta_z^6 + \mathrm{Sin}\,\theta_z^2\,\mathrm{Cos}\,\theta_z^4 + 2\mathrm{Sin}\,\theta_z^4\,\mathrm{Cos}\,\theta_z^2\right)\left(Q_{12}\alpha_1 + \frac{5}{8}Q_{22}\alpha_2\right)\end{array}\right\}.\left(z_k^{2'} - z_{k-1}^{2}{}'\right) \quad (17)$$

$$\left[\overline{M}_y^T\right] = \int_0^{2\pi} M_y^T * R_m.d\theta$$

$$= \int_0^{2\pi} \frac{\Delta T}{2}.\sum_{k=1}^{N}\left(\hat{Q}_{21}^k.\alpha_x^k + \hat{Q}_{22}^k.\alpha_y^k + \hat{Q}_{26}^k.\alpha_{xy}^k\right).\left[\left(\left(z'_k + R_m.\mathrm{Cos}\,\theta\right)^2 - \left(z'_{k-1} + R_m.\mathrm{Cos}\,\theta\right)^2\right)\right]R_m.d\theta$$

$$= \frac{\pi.R_m.\Delta T}{2}.\left\{\begin{array}{l}\left(\mathrm{Sin}\,\theta_z^6 + \mathrm{Sin}\,\theta_z^2\,\mathrm{Cos}\,\theta_z^4 + 2\mathrm{Sin}\,\theta_z^4\,\mathrm{Cos}\,\theta_z^2\right)\left(2Q_{11}\alpha_1 + \frac{3}{4}Q_{12}\alpha_2\right) + \\ \left(\mathrm{Cos}\,\theta_z^6 + \mathrm{Sin}\,\theta_z^4\,\mathrm{Cos}\,\theta_z^2 + 2\mathrm{Sin}\,\theta_z^2\,\mathrm{Cos}\,\theta_z^4\right)\left(Q_{12}\alpha_1 + \frac{5}{8}Q_{22}\alpha_2\right)\end{array}\right\}.\left(z_k^{2'} - z_{k-1}^{2}{}'\right)$$

$$\left[\overline{M}_y^H\right] = \int_0^{2\pi} M_y^H * R_m.d\theta$$

$$= \int_0^{2\pi} \frac{\Delta C}{2}.\sum_{k=1}^{N}\left(\hat{Q}_{21}^k.\alpha_x^k + \hat{Q}_{22}^k.\alpha_y^k + \hat{Q}_{26}^k.\alpha_{xy}^k\right).\left[\left(\left(z'_k + R_m.\mathrm{Cos}\,\theta\right)^2 - \left(z'_{k-1} + R_m.\mathrm{Cos}\,\theta\right)^2\right)\right]R_m.d\theta$$

$$= \frac{\pi.R_m.\Delta C}{2}.\left\{\begin{array}{l}\left(\mathrm{Sin}\,\theta_z^6 + \mathrm{Sin}\,\theta_z^2\,\mathrm{Cos}\,\theta_z^4 + 2\mathrm{Sin}\,\theta_z^4\,\mathrm{Cos}\,\theta_z^2\right)\left(2Q_{11}\alpha_1 + \frac{3}{4}Q_{12}\alpha_2\right) + \\ \left(\mathrm{Cos}\,\theta_z^6 + \mathrm{Sin}\,\theta_z^4\,\mathrm{Cos}\,\theta_z^2 + 2\mathrm{Sin}\,\theta_z^2\,\mathrm{Cos}\,\theta_z^4\right)\left(Q_{12}\alpha_1 + \frac{5}{8}Q_{22}\alpha_2\right)\end{array}\right\}.\left(z_k^{2'} - z_{k-1}^{2}{}'\right) \quad (18)$$

$$\left[\overline{M}_{XY}^{T}\right]=\int_{0}^{2\pi} M_{xy}^{T} * R_m.d\theta$$

$$=\int_{0}^{2\pi}\frac{\Delta T}{2}.\sum_{k=1}^{N}\left(\hat{Q}_{61}^{k}.\alpha_x^k+\hat{Q}_{62}^{k}.\alpha_y^k+\hat{Q}_{66}^{k}.\alpha_{xy}^k\right).\left[\left(\left(z'_k+R_m.\mathrm{Cos}\theta\right)^2-\left(z'_{k-1}+R_m.\mathrm{Cos}\theta\right)^2\right)\right]R_m.d\theta$$

$$=\frac{\pi.R_m.\Delta T}{2}.\begin{Bmatrix}\left(\mathrm{Sin}\theta\mathrm{Cos}\theta_z^5+\mathrm{Sin}\theta_z^5\mathrm{Cos}\theta_z+2\mathrm{Sin}\theta_z^3\mathrm{Cos}\theta_z^3\right)\left(2Q_{11}\alpha_1-Q_{12}\alpha_1\right)+\\ \left(\mathrm{Sin}\theta\mathrm{Cos}\theta_z^5+\mathrm{Sin}\theta_z^5\mathrm{Cos}\theta_z+2\mathrm{Sin}\theta_z^3\mathrm{Cos}\theta_z^3\right)\left(\frac{3}{4}Q_{12}\alpha_2-\frac{5}{8}Q_{22}\alpha_2\right)\end{Bmatrix}.\left(z_k^{2'}-z_{k-1}^{2\,'}\right)$$

$$\left[\overline{M}_{XY}^{H}\right]=\int_{0}^{2\pi} M_{xy}^{H} * R_m.d\theta \tag{19}$$

$$=\int_{0}^{2\pi}\frac{\Delta C}{2}.\sum_{k=1}^{N}\left(\hat{Q}_{61}^{k}.\alpha_x^k+\hat{Q}_{62}^{k}.\alpha_y^k+\hat{Q}_{66}^{k}.\alpha_{xy}^k\right).\left[\left(\left(z'_k+R_m.\mathrm{Cos}\theta\right)^2-\left(z'_{k-1}+R_m.\mathrm{Cos}\theta\right)^2\right)\right]R_m.d\theta$$

$$=\frac{\pi.R_m.\Delta C}{2}.\begin{Bmatrix}\left(\mathrm{Sin}\theta\mathrm{Cos}\theta_z^5+\mathrm{Sin}\theta_z^5\mathrm{Cos}\theta_z+2\mathrm{Sin}\theta_z^3\mathrm{Cos}\theta_z^3\right)\left(2Q_{11}\alpha_1-Q_{12}\alpha_1\right)+\\ \left(\mathrm{Sin}\theta\mathrm{Cos}\theta_z^5+\mathrm{Sin}\theta_z^5\mathrm{Cos}\theta_z+2\mathrm{Sin}\theta_z^3\mathrm{Cos}\theta_z^3\right)\left(\frac{3}{4}Q_{12}\alpha_2-\frac{5}{8}Q_{22}\alpha_2\right)\end{Bmatrix}.\left(z_k^{2'}-z_{k-1}^{2\,'}\right)$$

4. FINITE ELEMENT ANALYSIS OF RECTANGULAR AND CIRCULAR LAMINATED COMPOSITE BEAMS

A sixteen ply symmetric-balanced configuration with a $[+45/-45/90/0/90/0/+45/-45]_s$ stacking sequence is assumed to model the ply lay-up for this analysis . Table-1 illustrates the assumed material properties of AS4/3501-6 carbon-epoxy composite material system [21, 22, 23] utilized for conducting this study. A constant length of 40 inches long, 10 inches in width and a uniform cross-sectional thickness for the rectangular composite beam are assumed throughout the analysis. An ANSYS based geometrically linear FE analysis [24] is established to model and computationally simulate the structural response of a thin-walled, multi-directionally laminated composite beam configuration under hygrothermomechanical loading conditions.

Table 1. Material Properties for (AS4/3501-6) Carbon Epoxy [23]

Property	Value
E_{11}	$21.3*10^6$ psi
$E_{22}= E_{33}$	$1.5*10^6$ psi
$\upsilon_{12} = \upsilon_{13}$	0.27
υ_{23}	0.54
$G_{12}= G_{13}$	$1*10^6$ psi
G_{23}	$5.4*10^5$ psi
t_{ply}	0.005 inches
α_1	$-0.5*10^{-6}$ in/in/ ^oF
α_2	$15*10^{-6}$ in/in/ ^oF

Initial study essentially deals with the solid modeling and finite element analysis of a thin-walled, rectangular beam configuration. As shown in (Fig. 4), a 3-D volume schematic of the thin-walled beam construction is initially constructed upon extruding a generated 2-D area characterized by its cross-sectional properties. The model is further categorized as a Solid where the stacking arrangement is fed as a necessary input into the "sectional property" dialog box of the composite design interface [24].

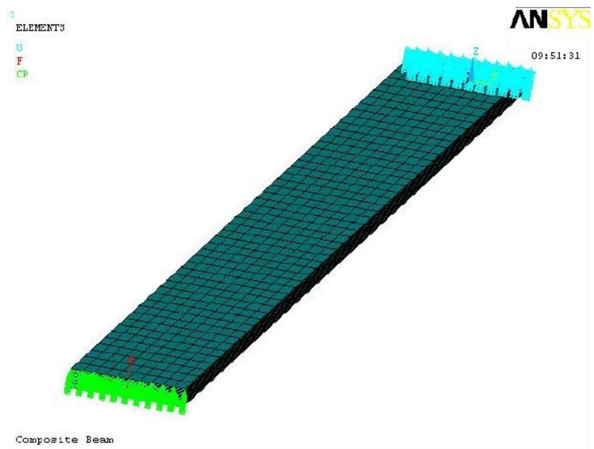

Fig.4. Discretized Rectangular Composite beam subject to Transverse Shear Load q

The 3D model shown in Fig. 4 is designed and modeled utilizing a SOLID 46 solid element [24], which is a 3D 8-node layered structural solid brick element. The element offers the ability to accurately model layered thick shells or solids and allows up to 250 various material layers. The element has three degrees of freedom on each node: translations on nodal x, y, and z directions. The model has a mesh density in the order of 6,400 8-node brick elements approximately totaling 7,667 nodes.

In this model, each element represents one layer of the laminate along the thickness direction. The beam is fixed across one boundary (right face) and free of any externally applied boundary conditions on the left face, thus simulating a cantilevered beam type configuration. All nodes on the built-in edge are constrained along all degrees of freedom thus preventing any translation or rotation of nodes under external loading. On the free edge, a transverse shear load of 10 lbs is applied along the z-axis (thickness direction, upward) to a massless point node that cohesively ties all the slave free-edge nodes to the master massless point node.

The massless point node (dummy node) is created and positioned in the center point of the laminate cross-sectional plane that bisects the laminate about the x and y-axis respectively (Fig. 4). By invoking the CP command [24] in ANSYS, all DOF associated with the slave nodes are seamlessly coupled to the Master massless dummy node. This feature essentially forces that portion of the model to behave as a rigid body.

4.1 In-plane Stress Evaluation in Rectangular Composite Beams Subject to Transverse Shear Loads

The in-plane stresses of the rectangular composite beam with temperature effect can be obtained by using the formulations developed earlier by Mahadev and Chan [1, 8, 10]. This beam is cantilevered in one end, and a transverse force, q = 10 lbs., is applied upward in the other end.

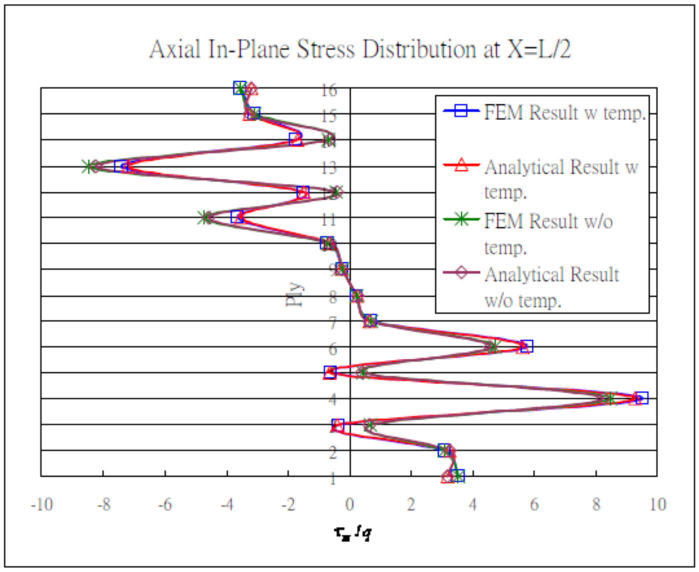

Fig.5. Normalized Longitudinal Stress Distribution across the Beam Thickness

Additionally, the stacking sequence of the laminate is $[\pm 45/90/0/90/0/\pm 45]_S$, and the temperature differential is assumed 50°F higher than the stress-free temperature (assumed to be at the room temperature). Fig. 5 depicts the axial stress distribution computed at the nodes across the thickness direction located at 50% length (to majorly alleviate edge effects). The comparison of the results between the analytical solution and finite element analysis is shown in Fig.5.

The axial stress profile computed through the laminate thickness indicates that the distribution is discontinuous yet symmetric (tension and compression) with respect to the mid-lamina in the absence of a temperature differential. On the contrary, the axial stress profile displays a discontinuous unsymmetrical distribution (tension and compression) across the height of the laminate in the presence of 50^0 F temperature differential. Additionally, the outer 0 deg ply experience a higher thermally induced stress as opposed to the inner 0 deg ply within the laminate. The deformation and the contour plot of the axial stress distribution of the composite beam are shown in Fig. 6.

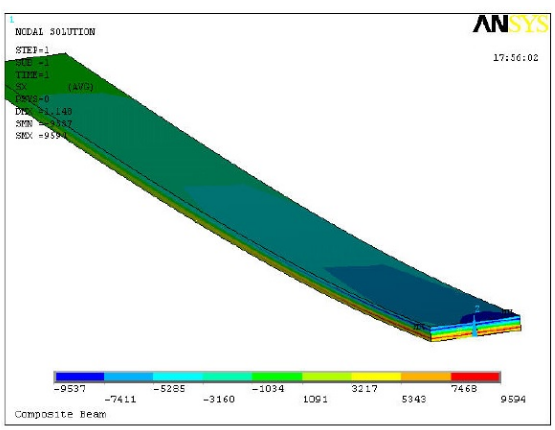

Fig.6. Contour Plot of Axial In-plane Stress Distribution in Composite Beam

Based on this research, it was discovered that the hygrothermal forces and moments do not affect the distribution of interlaminar shear stresses in a thin-walled rectangular composite beam that is cantilevered in one end and subject to a transverse shear load in the other end. The transverse load, q here is assumed to be 1 lb/in, and the laminate is composed of a [±45 / 90 / 0 / 90 / 0 /± 45]*S* lay-up. Further, 50 °F temperature differential is assumed. Fig. 7 shows a comparison of the results between the FEM model and the analytical model and shows excellent agreement.

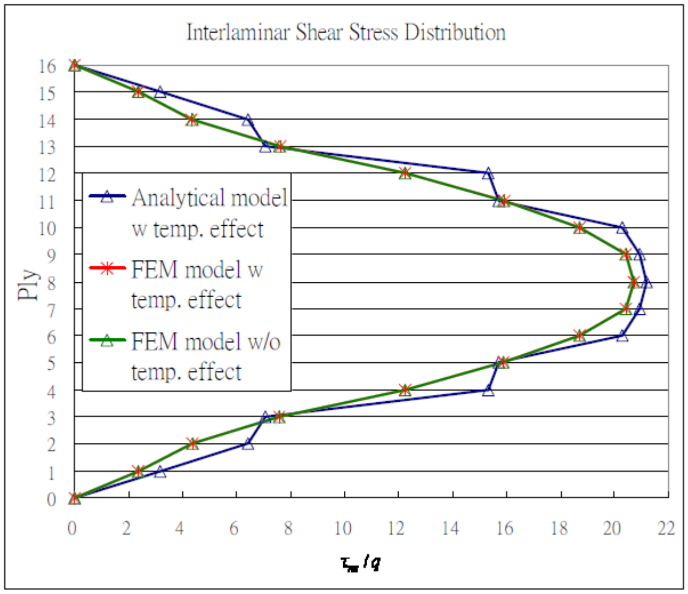

Fig.7. Normalized Interlaminar Shear-stress Distribution in Composite Beam

The interlaminar shear stress profile shows that the plies located in the extremities experience no interlaminar shear stresses and the innermost plies in proximity to the laminate mid-plane. The distribution is primarily bell-shaped. There is no magnitude change in the interlaminar shear stress distribution under a temperature differential.

4.2 In-plane Stress Evaluation in Tubular Laminated Composite Beams Subject to Transverse Shear Loads

A sixteen ply symmetric-balanced configuration with a $[+45/-45/90/0/90/0/+45/-45]_s$ stacking sequence is assumed to model the ply lay-up for this tubular beam analysis. Table-1 illustrates the assumed material properties of AS4/3501-6 carbon-epoxy composite material system [23] utilized for conducting this study. A constant length of 20 inches long, 1 inch mean radius, and a uniform cross-sectional thickness for the circular composite beam are assumed throughout the analysis. An ANSYS based geometrically linear FE analysis [24] is established to model and computationally simulate the structural response of a thin-walled, multi-directionally laminated composite beam configuration under hygrothermomechanical loading conditions.

Second phase of the FEA study essentially deals with the solid modeling and finite element analysis of a thin-walled, tubular beam configuration. As shown in (Fig. 7), a 3-D volume schematic of the thin-walled beam construction is initially constructed upon extruding a generated 2-D area characterized by its cross-sectional properties. The model is further categorized as a Solid where the stacking arrangement is fed as a necessary input into the "sectional property" dialog box of the composite design interface [24]. The 3D model shown in Fig. 8 is designed and modeled utilizing a SOLID 46 solid element [24], which is a 3D 8-node layered structural solid brick element. The element offers the ability to accurately model layered thick shells or solids and allows up to 250 various material layers. The element has three degrees of freedom on each node: translations on nodal x, y, and z directions. The model has a mesh density in the order of 11,520 eight-noded brick elements approximately totaling 12,852 nodes. In this model, each element represents one layer of the laminate along the thickness direction. The beam is fixed across one boundary (right face) and free of any externally applied boundary conditions on the left face, thus simulating a cantilevered beam type configuration. All nodes on the built-in edge are constrained along all degrees of freedom thus preventing any translation or rotation of nodes under external loading. On the free edge, a transverse shear load of 10 lbs. is applied along the z-axis (thickness direction, upward) to a massless point node that cohesively ties all the slave free-edge nodes to the master massless point node. The massless point node (dummy node) is created and positioned in the center point of the laminate cross-sectional plane that bisects the laminate about the x and y-axis respectively (Fig. 4). By invoking the CP command [24] in ANSYS, all DOF associated with the slave nodes are seamlessly coupled to the Master massless dummy node. This feature essentially forces that portion of the model to behave as a rigid body.

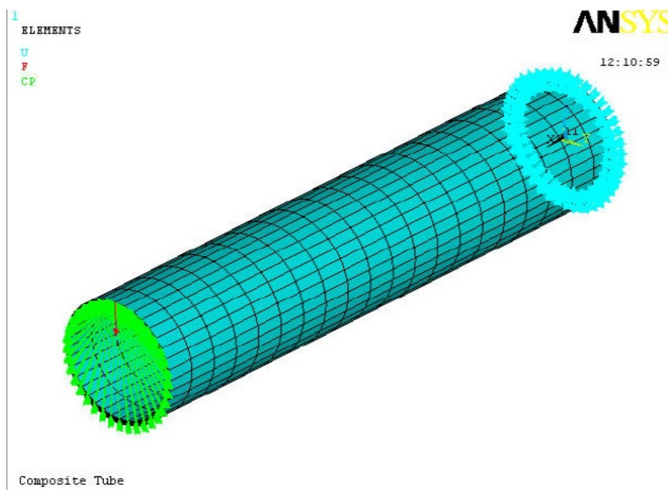

Fig.7. Discretized Tubular Composite beam subject to Transverse Shear Load q=10 lbs

The following investigation presents the results for the in-plane stress distribution in the laminated composite tube along the axial direction (x-direction) under temperature environment. Figures 8 through 11 show the in-plane stress contour along the circumferential direction for 45° , − 45° , 90° , and 0° plies in the presence and absence of a uniform temperature differential respectively. It can be observed that the magnitude of axial stress acquired through FEA passes through a state of zero stress for circumferential points located along the global neutral axis (90 degrees and 270 degrees) respectively. Under the presence of a finite thermal loading of , composite tubular beam exhibits a significant increase in longitudinal stresses along the circumference and stress magnitudes based at circumferential (90 deg and 270 deg) locations indicate finite non-zero stresses.

Longitudinal stresses computed analytically utilizing the concept of Layered stress recovery is also shown in Figs. 8 through 11. 0-deg ply stresses determined by including and excluding thermal effects collapse onto each other indicating excellent agreement and validity between these distinct approaches. Fig. 8 and Fig.9 represents the longitudinal stress plots for the +45 deg plies and -45 degree plies as a function of the circumferential angle of the tubular beam. Stress profiles indicate smaller stress magnitudes as opposed to 0 deg plies that are primarily located along the length of the tube. Stress distribution curves for +45 deg and -45 deg plies obtained analytically, show only a small variation along the circumference in relation to the FEA based stress plots. Stress magnitudes for the 90 deg plies are the least and do not participate in carrying axial stresses.

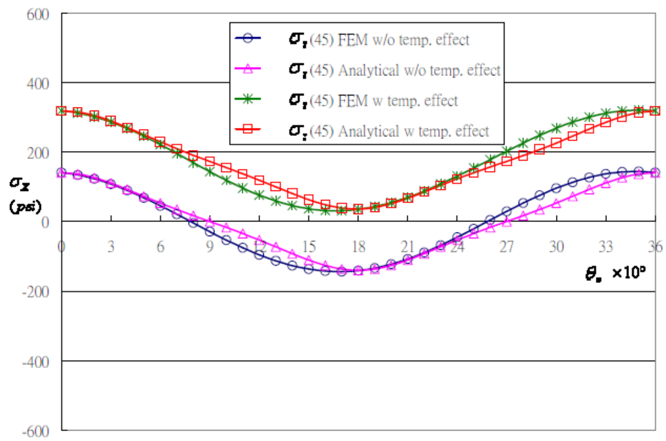

Fig.8. Longitudinal Stress Profile for +45 deg ply under Transverse Shear as a fn. of Circumferential Angle

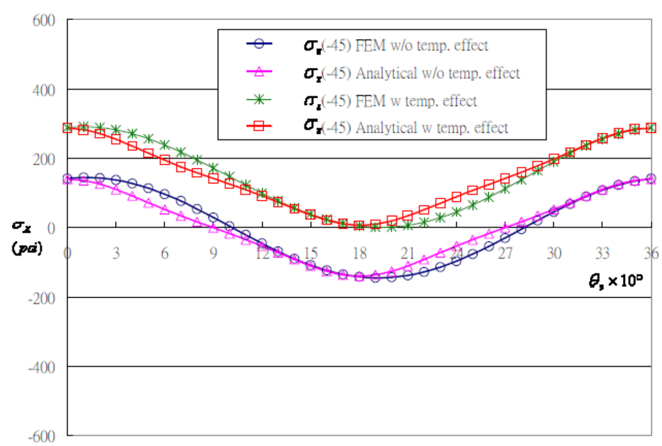

Fig.9. Longitudinal Stress Profile for -45 deg ply under Transverse Shear as a fn. of Circumferential Angle

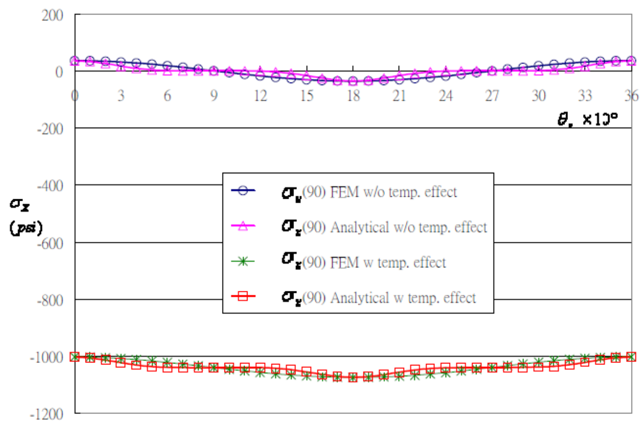

Fig.10. Longitudinal Stress Profile for 90 deg ply under Transverse Shear as a fn. of Circumferential Angle

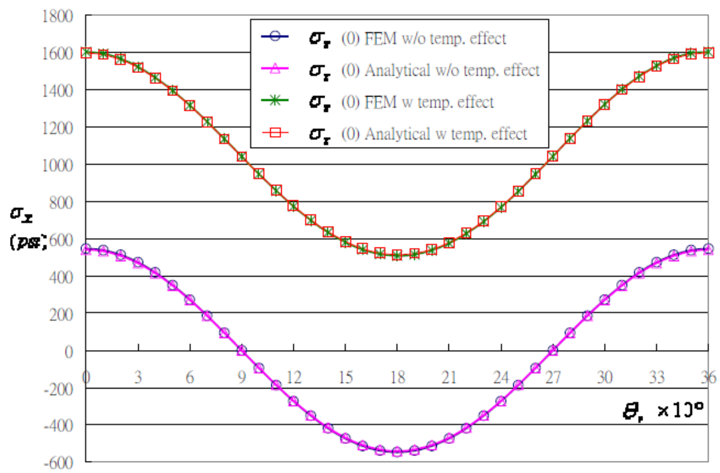

Fig.11. Longitudinal Stress Profile for 0 deg ply under Transverse Shear as a fn. of Circumferential Angle

4.3 Parametric Investigations on Rectangular and Tubular Composite Beams

This section showcases a preliminary parametric study that explores the effects of laminate stacking sequence and fiber orientation angle on thin-walled rectangular and circular composite beams. To examine the stacking sequence effects under the presence and absence of a temperature differential, three laminates with the same fiber orientations, but different stacking sequences are considered. $[\pm45 / 90 / 0 / 90 / 0 /\pm 45]_s$, $[+45/-45/ 90_2/+45/-45/0_2]_s$, and $[\pm45/ 90_2 /\pm 45/ 0_2]_{2T}$ are the three different lay-ups chosen for this study. The various results of the in-plane stresses for these three cases are observed.

Analytical results are shown for rectangular and tubular composite beams constituting the three aforementioned stacking sequences. Fig. 12 through Fig. 14 represents the through-thickness axial stress distribution of stresses. It is shown that the stress variation is symmetric (tension and compression) about the mid-plane for the two symmetric laminate stacking sequences as opposed to the unsymmetrical laminate stacking sequence applied to the rectangular composite beam analysis. 90 deg plies experience the least amount of stresses while the 0 deg plies accommodate the largest stress magnitudes.

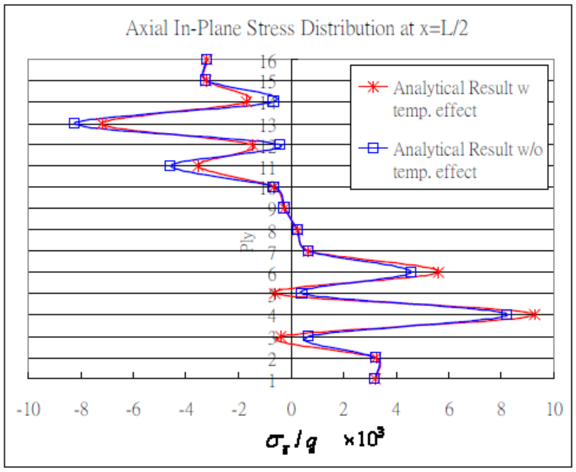

Fig.12. Normalized Axial Stress Distribution for [±45 / 90 / 0 / 90 / 0 /± 45]$_S$ Lay-up

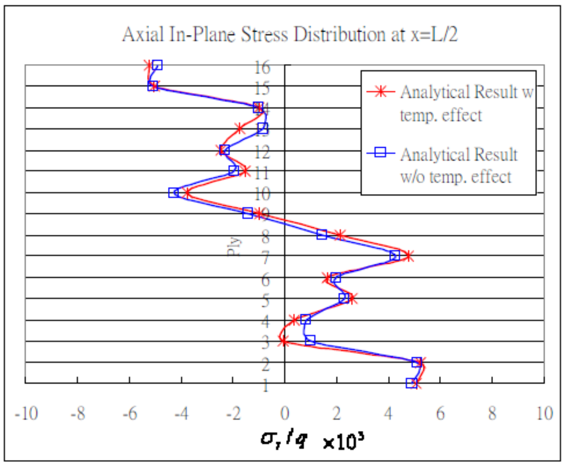

Fig.13. Normalized Axial Stress Distribution for [±45/ 90/90 /± 45/ 0/0]$_S$ Lay-up

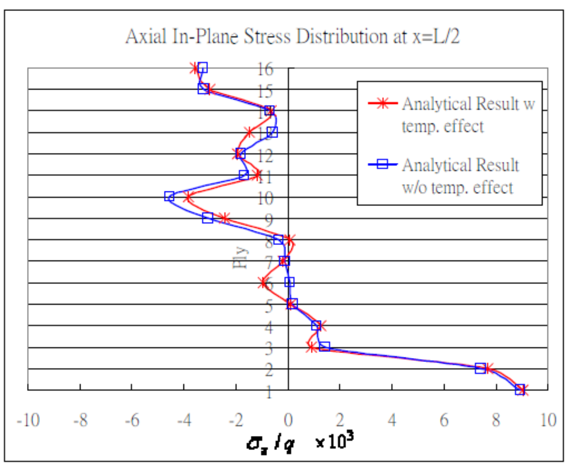

Fig.14. Normalized Axial Stress Distribution for [±45/ 90/90 /± 45/ 0]$_{2T}$ Lay-up

Fig.15 through Fig.17 represents the through-thickness axial stress distribution for tubular composite beams subject to three different laminate stacking sequences that have identical fiber angle orientations.

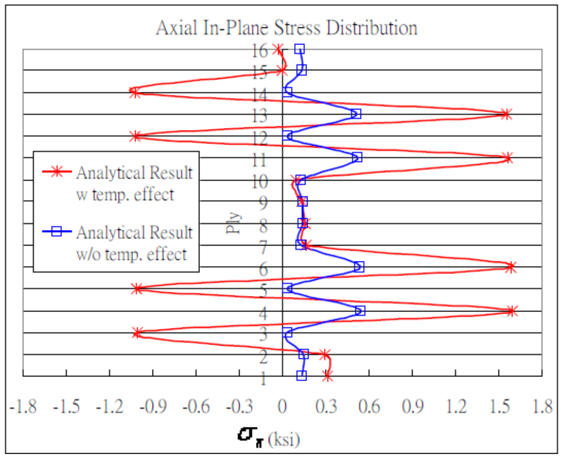

Fig.15. Normalized Axial Stress Distribution for [±45 / 90 / 0 / 90 / 0 /± 45]$_S$ Lay-up

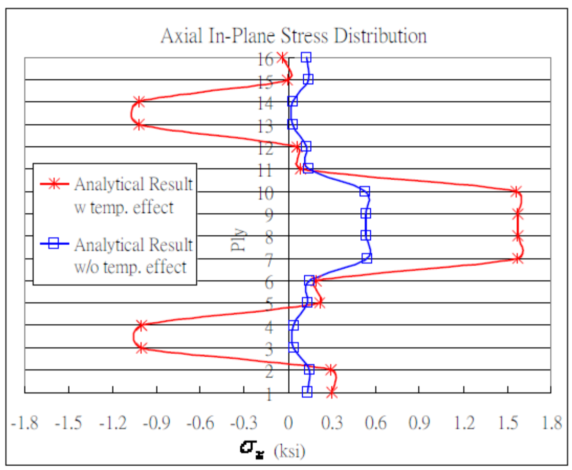

Fig.16. Normalized Axial Stress Distribution for [±45/ 90/90 /± 45/ 0/0]$_S$ Lay-up

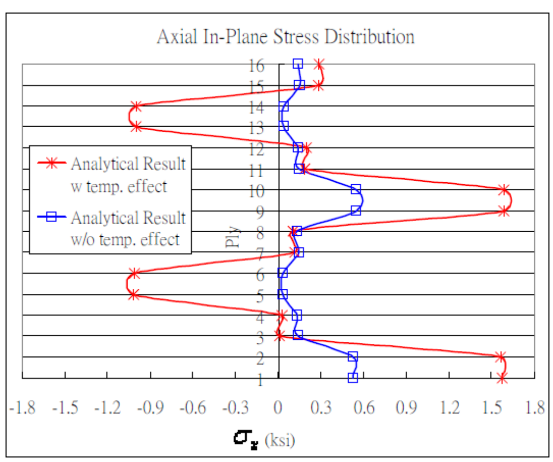

Fig.17. Normalized Axial Stress Distribution for [±45/ 90/90 /± 45/ 0]$_{2T}$ Lay-up

The directional dependence of a laminated composite material is one of the important properties in the design of the composite structure. To examine the fiber orientation angle effects under the presence and absence of a temperature differential, four fiber orientations; Four symmetric layups with ±θ ° and 0° are considered. 60°, 70°, 80°, and 90° are chosen as the value of fiber orientations of the laminate. The following figures represent the axial in-plane stresses of the tubes with these four different fiber orientations. The various results of the in-plane stresses for these four cases are observed. Analytical results are shown for tubular composite beams constituting the four aforementioned fiber orientations. Fig. 18 through Fig. 21 represents the through-thickness axial stress distribution of stresses. It is shown that the stress variation is symmetric about the mid-plane (8^{th} ply) for the all the lay-ups. The influence of the temperature differential is shown to have an increasing effect by incrementing the ±θ ° ply closer to 90 degrees. Table 2 indicates that the fiber orientation of the laminate plays an important role in the thermal induced in-plane stresses. From the results, it is seen that the Stacking sequence case involving 0° and 90° plies exhibits the greatest thermal effect in axial stress variation.

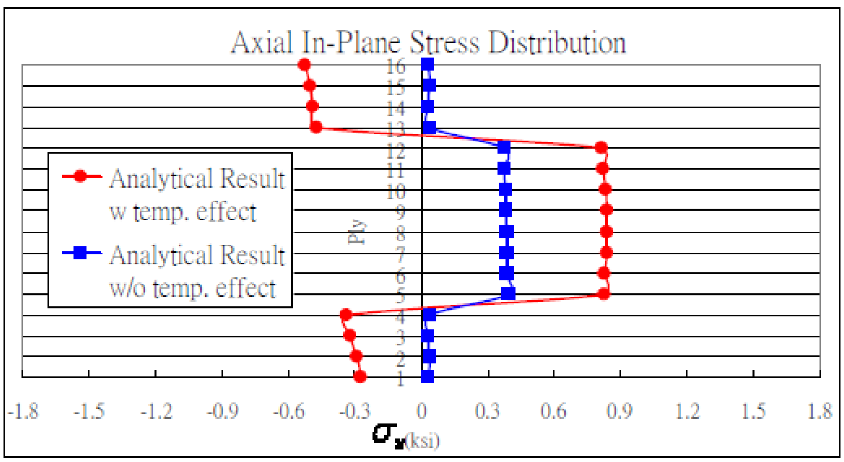

Fig.18. Axial Stress Distribution for distribution for tube with [$\pm 60_2$ / 0_4]s lay-up.

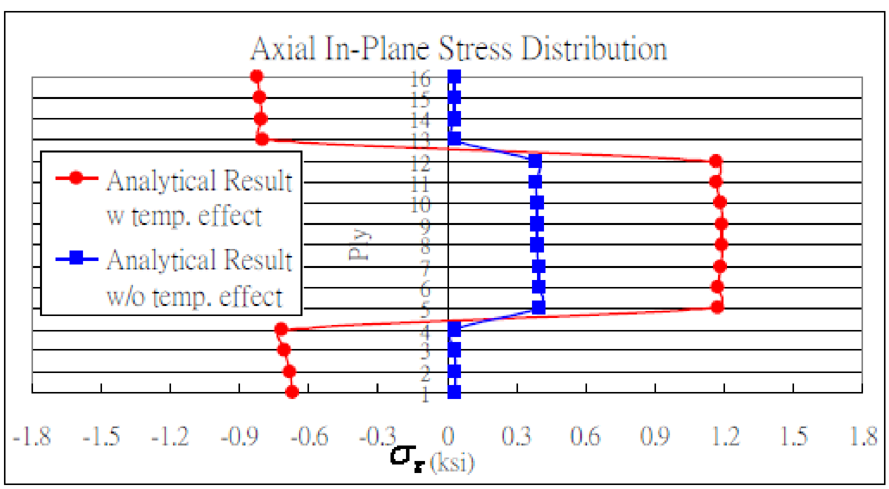

Fig.19. Axial Stress Distribution for distribution for tube with [$\pm 70_2$ / 0_4]s lay-up

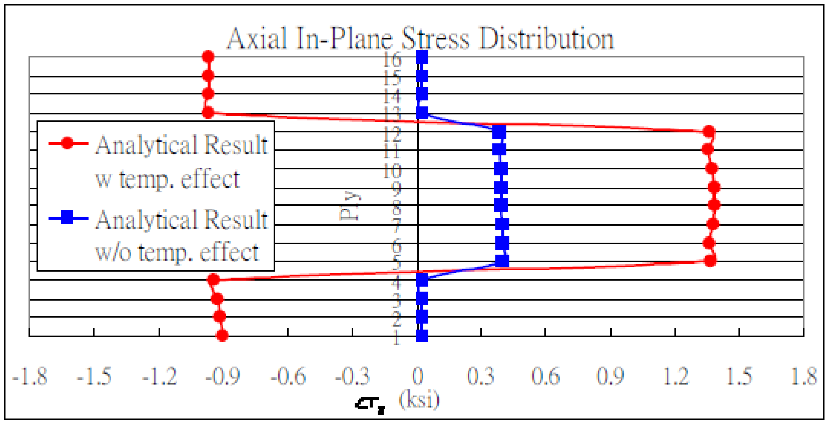

Fig.20. Axial Stress Distribution for distribution for tube with [±80₂ / 0₄]s lay-up

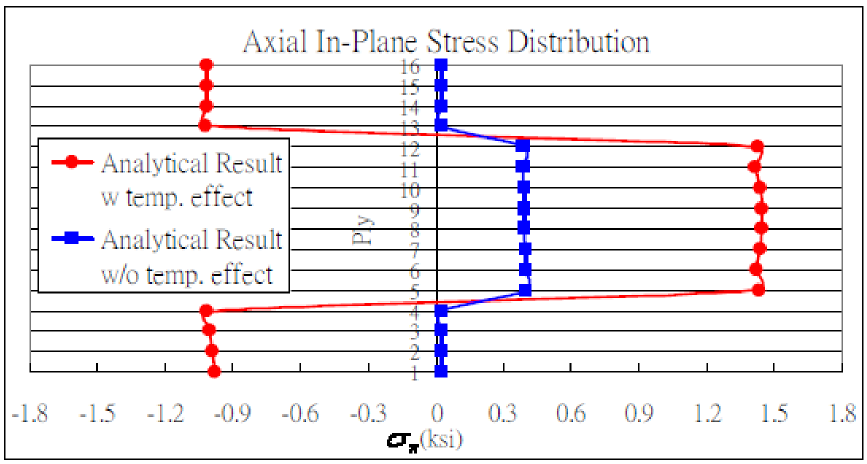

Fig.21. Axial Stress Distribution for distribution for tube with [±90₂ / 0₄]s lay-up

Table 2. Comparison of increased stresses in 0° ply due to thermal effect

Stacking sequence	Max. tensile stress with thermal effect	Max. tensile stress w/o thermal effect	Increased in-plane stress due to thermal effect
$[\pm 60_2/0_4]_S$	841.39 psi	393 psi	448.39 psi
$[\pm 70_2/0_4]_S$	1190.6 psi	399.1 psi	791.5 psi
$[\pm 80_2/0_4]_S$	1385.9 psi	401.18 psi	984.72 psi
$[\pm 90_2/0_4]_S$	1448.1 psi	401.69 psi	1046.41 psi

5. CONCLUSION

This work fundamentally describes the analytical development of simple closed-form mathematical formulations for accurately predicting the interlaminar shear stresses and longitudinal ply-stress variations that govern the extension-bend type mechanical response in thin-walled tubular and rectangular composite strip configurations respectively. A novel closed-form constitutive relationship for closed laminated beam structures subjected to mechanical and hygrothermal load environments are formulated. The global stiffness model (associated with relating resultant load matrices to mid-plane strains and curvatures) is initially constructed by utilizing extended Lamination theory principles (incorporating the mechanics of Classical Lamination Theory, transformation matrices and concepts of parallel-axes theorem) for describing the mechanical characteristics of a cylindrical composite beam system distinguishable by varying key parameters such as mean radius of curvature, circumferential arc length, ply-lay-up, laminate stacking sequence etc. The constitutive relationship recognizes the emergence of additional hygrothermal loads (forces and moments).

The novel constitutive relationship developed earlier in this research for studying composite tube configurations [1,8,10] is extended to analyze the hygrothermomechanical behavior of tubular and rectangular composite beam structures. Excellent agreement is shown in analytical centroid predictions in comparison to FEM based results (ANSYS). Analytical estimations for structural stiffness and in-plane stress distributions via Layer Stress Recovery indicated very good agreement with a percentage error difference of less than 3% as opposed to finite element predictions.

Analytical closed-form expressions to analyze thermal induced stresses for laminated composite beams with rectangular and tubular cross-sections were developed. All derivations were based on the modification of conventional lamination theory by using parallel axis theorem. For the circular composite tube, the stiffness matrices and thermal induced loads and moments were derived. The variation of stiffness along the contour is included. For rectangular beam, the narrow width of the beam is considered. All results of thermal stresses obtained from the analytical model were compared with results obtained from finite element model built with the commercial software package, ANSYS. From this study, the following conclusions can be made:

For cantilevered composite beams with a rectangular cross-section, we have

The axial in-plane stresses of each ply obtained by the current developed method exhibit an excellent agreement with the results obtained from finite element analysis. The interlaminar shear stresses of each ply calculated from the present method are in a good agreement with the results obtained from finite element analysis. The interlaminar shear stress due to the transverse load does not appear to have any influence by the presence of uniform temperature. While the set of plies is given, the stacking sequence of the laminate does not significantly affect the increased axial in-plane stress of the rectangular beam due to the thermal effect.

For cantilevered composite beams with a tubular cross-section, we obtain

The thermally induced stresses obtained by the present method give an excellent agreement with the finite element results. The fiber orientation of the plies plays an important role on the thermal induced in-plane stresses. This is chiefly contributed by the thermal induced moments. The induced moments are due to the mismatch of the axial thermal expansion between each ply of the laminate.

It is well understood that the analysis of moisture effect for a laminated beam is analogous to the thermal effects that influence the mechanical response of such structures. Hence, the present method is also applicable for the analysis of hygric effect of laminated composite structures.

6. REFERENCES

1. Mahadev, S., and Chan Wen., 2013. “Closed-Form Analytical Method for Analyzing Laminated Composite Tubes in Hygrothermal Environment”, Proceedings of the 54th AIAA/ASME/ASCE/AHS/ASC Structures, Structural Dynamics, and Materials Conference, Boston, USA, April 8-13, 2013.
2. J.M Whitney and C.T. Sun., “A Refined Theory for Laminated Anisotropic Cylindrical Shells”, J. of Applied Mechanics. Vol: 3, pp: 41-47, April 1984.
3. Whitney, J. M., and Leissa, A. W., "Analysis of Heterogeneous Anisotropic Plates", Journal of Applied Mechanics, Vol. 36, pp: 261-266, 1979.
4. Vinson, Sierakowski, M.J.,. “An Efficient higher-order shell theory for laminated composites”. Journal of Compos Struct; Vol: 34(2); pp: 197–212; 1996.
5. Vinson, Sierakowski, M.J.,. “An Efficient higher-order shell theory for laminated composites”. Journal of Compos Struct; Vol: 34(2); pp: 197–212; 1996.
6. Hoa, S.V., Analysis for Design of Fiber Reinforced Plastic Vessels and Piping, Technomic Publishing Co., Inc., 1991.
7. Librescu, L. and Song, O., Thin-Walled Composite Beams: Theory and Application, Springer Co., Inc., 2006.
8. Mahadev, S., and Chan Wen., 2015. “Closed-Form Analytical Solutions for Thin-Walled Cylindrical Composite Shells Structures Subjected to Axial and Bending Loads Under Temperature Environment”, Proceedings of the ASME 2015 International Engineering Congress and Exposition IMECE 2015, Houston, USA, November 13-19, 2015.
9. Chan, W.S. and Demirhan, K.C., “A Simple Closed-Form Solution of Bending Stiffness for Laminated Composite Tube”, Journal of Reinforced Plastics and Composites, v 19, No. 04, 2000, p 278-291.
10. Mahadev, S., and Hanze Zachary., 2017. “Analytical Treatment for Centroid Location Determination in Thin-walled Multidirectional Composite Shells”, SAMPE Conference Proceedings. Seattle, WA, May 22-25, 2017. Society for the Advancement of Material and Process Engineering-North America.
11. Roa, C.S., “Analysis of Tapered Laminated Composite Tubes under Tension and Torsion”, Master’s Thesis, University of Texas at Arlington, May 2007.
12. Sims, D.F. and Wilson, H.E., “Distribution of Shearing Stresses in a Composite Beam under Transverse Loading”, Composites, July 1978, p 185-191.
13. Syed, K.A. and Chan, W.S., “Analysis of Hat-Sectioned Reinforced Composite Beams”, Proceedings of American Society of Composites, Sept. 2006.
14. Boley, B.A. and Weiner, J.H., 1997, *Theory of Thermal Stresses*, Dover Publications, INC., Mineola, NY.
15. Naidu, N.V.S. and Sinha, P.K., “Nonlinear Finite Element Analysis of Laminated Composite Shells in Hygrothermal Environment”, Composites Structures, v 69, 2005,p 387-395.

16. Seibi, A.C. and Amatcau, M.F., “Finite Element Modeling and Optimization for Controlling the Residual Thermal Stresses of Laminated Composite Tubes”, Composite Structures, v 41, 1998, p 151-157.

17. Shariyat, M., “Thermal Buckling Analysis of Rectangular Composite Plate with Temperature-Dependent Properties based on a layer-wise theory”, Thin-Walled Structures, v 45, 2007, p 439-452.

18. Kim, B.-S., Kim, T.-W., Byun, J.-H., and Lee, W.-I., “Stress Analysis of Composite/Ceramic Tube Subjected to Shrink Fit, Internal Pressure and Temperature Differences.” Key Engineering Materials, v 137, 1998, p 32-39.

19. Khdeir, A. A., “Thermal Buckling of Cross-Ply Laminated Composite Beam.” ACTA Mechanica, v 149, n 1-4, 2001, p 201-213.91

20. Syed, K.A., Su, C.W., and Chan, W.S., “Analysis of Fiber Reinforced Composite Beams under Temperature Environment”, Proceedings of the Seventh International Congress on Thermal Stresses, Taipei, Taiwan, 2007.

21. Gay, P. and Hoa, S.V., 2007, *Composite Material Design and Applications second edition*, CRC Press.

22. Tuttle, M.E., Chapter 5 and 6 in *Structural Analysis of Polymeric Composite Materials*, Marcel Dekker, INC., New York, NY.

23. Daniel, I.M. and Ishai, O., 2006, Chapter 7 and 8 in *Engineering Mechanics of Composite Material second edition*, Oxford University Press, INC., New York, NY.

24. ANSYS 18.0, Technical User’s Manual.